Forces between like-charged plates in electrolyte solution: Ion-solvent packing versus electrostatic effects

Frank Otto and G. N. Patey
Department of Chemistry, University of British Columbia, Vancouver, British Columbia, Canada V6T 1Z1
(Received 12 February 1999)

The anisotropic hypernetted-chain approximation is solved numerically for mixtures of neutral hard-sphere solvent particles and divalent counterions between charged plates. A detailed analysis of the different components of force acting between the plates is given. At separations of a few solvent diameters, it is shown that even at relatively high surface charge and moderate solvent density, the ionic contribution to the force tends to be dominated by the hard-core or packing component. If the ions and solvent particles are of equal size, then the net pressure between the plates can be reasonably well approximated by adding the pressures of pure one-component ionic and solvent systems. However, if the ion and solvent diameters are significantly different the pressure curve is more complex, and the simple superposition of the ionic and solvent pressures no longer works. For this case, we show that to a good approximation it is still possible to divide the pressure into electrostatic and hard-core components, but now the appropriate hard-core system must itself be a mixture of neutral hard spheres. [S1063-651X(99)08210-0]

PACS number(s): 68.45.−v, 61.20.Gy, 61.20.Qq, 82.45.+z

I. INTRODUCTION

The average force acting between like-charged macroparticles in electrolyte solutions plays a fundamental role in determining the behavior of colloidal systems. These forces depend on details of the interacting double layers and sometimes the results can be rather unexpected. For example, it is now well established [1,2] that like-charged plates immersed in a primitive model (PM) (i.e., continuum solvent) solution with divalent counterions can experience an attractive interaction at short range, contrary to the predictions of the classical Poisson-Boltzmann theory. This is a very interesting observation, however, in real electrolyte solutions solvent effects not included in the PM might be important and may even dominate the electrostatic contribution at smaller wall-wall separations. This is an important question which deserves further attention and some aspects of discrete solvent effects are addressed in this paper.

While it is now possible [3] to examine bulk electrolyte solutions using quite realistic solvent models and reasonably accurate theories, the same level of treatment is not yet feasible for inhomogeneous systems. Therefore, investigations of two interacting double layers have usually employed the PM, where the ions are represented by charged hard spheres and the solvent is a dielectric continuum without any inherent granularity. We would expect discrete solvent effects to alter the PM results through at least two mechanisms. These are particle packing constraints and the relative lack of dielectric screening at small ion-ion and ion-wall separations. The latter effect comes about as the description of the solvent as a continuum with a distance independent dielectric constant begins to break down; for example, in an ''associated'' pair the ion-ion interaction is much stronger than the PM would imply. It might be possible to include the reduced dielectric screening effects by employing McMillan-Mayer level theory with effective ion-ion and ion-wall interactions [4]. However, in the present paper we focus upon solvent granularity and its effects on the ion distributions and on the force between immersed charged walls. It has been proposed [5,6] that the net pressure between plates in an ion-solvent mixture might be given, at least approximately, by the superposition of separate ion and solvent contributions obtained from simpler one-component models. An important objective of the present work is to examine the validity of this appealing suggestion.

Some related earlier work has been reported by Davis and co-workers [7–9] and by Patra and Ghosh [10]. These authors considered ions in hard-sphere solvents using the methods of density functional theory. They found that at high density the pressure between plates exhibited an oscillatory structure due to the hard-core interactions. In the present paper we consider similar models but employ anisotropic integral equation techniques which are known to be quite accurate for inhomogeneous systems. However, our main purpose is not to compare results obtained by different theoretical methods, but rather to complement the earlier findings with a detailed analysis of the fluid structure and, particularly, of the net pressure in terms of its component parts. Cases where the ions and solvent particles are of equal and unequal size are discussed.

The remainder of the paper consists of three parts. The model and methods are described in Sec. II, the results are presented in Sec. III, and our conclusions are summarized in Sec. IV.

II. THE MODEL AND NUMERICAL METHOD

The system considered consists of two infinite parallel hard walls at a separation d_{wall} which are homogeneously charged with a surface charge density $\sigma=-0.267$ C/m^2 $=1e/60$ Å^2. The fluid between the walls is a mixture of hard-sphere counterions and neutral hard-sphere solvent particles. The diameters of the ions and solvent particles are d_{ion} and d_{hs}, respectively. Two particles at a distance R interact via the pair potential

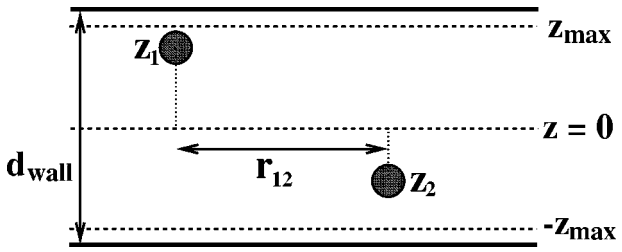

FIG. 1. The frame of reference used in the calculations.

$$u_{ij}(R)=u_{ij}^{\mathrm{hs}}(R)+u_{ij}^{\mathrm{el}}(R)=\begin{cases}\infty & \text{if } R<\dfrac{1}{2}(d_i+d_j)\\ \dfrac{q_i q_j}{4\pi\epsilon_0\epsilon R} & \text{otherwise,}\end{cases} \tag{2.1}$$

where ϵ is the dielectric constant, ϵ_0 is the vacuum permittivity, and q_i denotes the charge associated with particle i.

We employ the reference frame shown in Fig. 1 with coordinates z and $r=\sqrt{x^2+y^2}$, where $z=0$ designates the midplane between the walls. The planes of closest approach to the walls for particle type i are defined by $z=\pm z_{\mathrm{max},i}$, $z_{\mathrm{max},i}=(d_{\mathrm{wall}}-d_i)/2$. To obtain the particle density profiles $\rho_i(z)$ and particle distribution functions $g_{ij}(r_{12},z_1,z_2)$, we employ the formalism of anisotropic integral equations which has been extensively used by Kjellander and coworkers [1,5,11–16] among others. The theory and method of numerical solution are well established and we restrict our discussion to a short outline.

The Ornstein-Zernike equation relates the direct correlation function $c_{ij}(r_{12},z_1,z_2)$ to the pair correlation function $h_{ij}(r_{12},z_1,z_2)=g_{ij}(r_{12},z_1,z_2)-1$ and $\rho_i(z)$ such that

$$h_{ij}(r_{12},z_1,z_2)=c_{ij}(r_{12},z_1,z_2)+2\pi\sum_k \int r_3 dr_3 dz_3 \times c_{ik}(r_{13},z_1,z_3)\rho_k(z_3)h_{kj}(r_{32},z_3,z_2). \tag{2.2}$$

A convenient closure for Eq. (2.2) is the hypernetted-chain (HNC) approximation

$$h_{ij}(r_{12},z_1,z_2)=\exp[-\beta u_{ij}(R_{12})+h_{ij}(r_{12},z_1,z_2)-c_{ij}(r_{12},z_1,z_2)]-1, \tag{2.3}$$

where $R_{12}=\sqrt{r_{12}^2+(z_1-z_2)^2}$ and $\beta=(k_BT)^{-1}$. This yields excellent results for systems that are dominated by Coulombic interactions at low to medium densities [2]. On the other hand, it is well known that the HNC approximation does not perform comparatively well for dense homogeneous liquids with short-range pair potentials, and this holds true for the inhomogeneous case as well. However, this limitation in the treatment of the hard-core interactions does not seriously affect our conclusions as much of the discussion is qualitative in nature, and all quantitative comparisons are made between systems involving the same level of approximation.

The HNC approximation is advantageous since it yields an easy way to calculate the density profiles once the activities a_i for the solution between the walls are known. One has

$$\rho_i(z_1)=a_i\exp\Big(-\beta v_i(z_1)+\tfrac{1}{2}[h_{ii}(0,z_1,z_1)-c_{ii}(0,z_1,z_1)] -2\pi\sum_j \int r_{12}dr_{12}dz_2\,\rho_j(z_2)\,[\tfrac{1}{2}h_{ij}^2(r_{12},z_1,z_2) -c_{ij}(r_{12},z_1,z_2)]\Big), \tag{2.4}$$

where $v_i(z)$ is the particle-wall potential energy with $v_i(z)=\infty$, if $|z|>\frac{1}{2}(d_{\mathrm{wall}}-d_i)$. The average ion density is dictated by the electroneutrality condition between the plates, $2\sigma+q_{\mathrm{ion}}\int\rho_{\mathrm{ion}}(z)dz=0$, and no electrolyte solution outside the cavity is taken into account. The advantage of this procedure lies in the restriction to a two-component mixture which is much easier to treat than the full three-component model. While this simplified model clearly involves some level of physical approximation, it provides a reasonable description of the situation for highly charged plates immersed in dilute electrolyte solution [2].

The system of equations is solved self-consistently by first iterating Eqs (2.2) and (2.3) for an initial set of density profiles until successive iterations of the correlation functions do not differ more than 0.1%. Obtaining the new $\rho_i(z)$ from Eq. (2.4), the loop is repeated until successive density profiles change less than 0.01%. Following Kjellander [14], we note that by using a two-dimensional Fourier transform (Hankel transform) for the correlation functions in each layer (see below) the three-dimensional integral in Eq. (2.2) can be transformed into a one-dimensional integral which is much easier to solve. Thus, we have to perform two transformations in every iteration loop for which no ''fast-Fourier-transform- (FFT-) like'' algorithm is known [17]. Also, due to the discontinuity of $c_{ij}(r_{12},z_1,z_2)$ and $h_{ij}(r_{12},z_1,z_2)$ at hard-core contact, the Fourier transforms have long-range tails which can be avoided by adding an appropriate second order polynomial to the function in r space and subtracting the corresponding analytically known tail in Fourier space [14].

For all particle types the space between the plates is partitioned into up to 81 parallel layers of which the wall layers are particularly thin. Parallel to the wall we use 300 grid points with a cutoff, $r_{\mathrm{max}}=7\,d_{\mathrm{hs}}$, beyond which we set $h_{ij}(r_{12},z_1,z_2)=0$ and $c_{ij}(r_{12},z_1,z_2)=-\beta u_{ij}^{\mathrm{el}}(\sqrt{r_{12}^2+(z_1-z_2)^2})$, the latter choice equating c_{ij} with its asymptotic value. These long-range tails are handled analytically throughout the calculation. The terms in Eq. (2.4) involving $v_i(z)$ and the asymptotic part of c_{ij}, $-\beta u_{ij}^{\mathrm{el}}$, have to be evaluated together to yield the finite result [12]

$$-\beta v_{\mathrm{ion}}(z_1)-2\pi\int r\,dr\,dz_2\,\rho_{\mathrm{ion}}(z_2) \times\beta u_{\mathrm{ion\,ion}}^{\mathrm{el}}[\sqrt{r^2+(z_1-z_2)^2}] =\frac{\beta q_{\mathrm{ion}}}{2\epsilon\epsilon_0}\Big[\sigma d_{\mathrm{wall}}+q_{\mathrm{ion}}\int dz_2|z_1-z_2|\rho_{\mathrm{ion}}(z_2)\Big]. \tag{2.5}$$

We carefully checked to ensure that our results are independent of the number of layers, grid points, and r_{max}.

We now briefly summarize how the perpendicular component of the pressure tensor (i.e., the pressure between the walls) is calculated. Carnie and Chan [18] have derived contact theorems for a number of model electrolytes. For our case, the contact theorem takes the well-known form

$$P_{\text{slit}} = k_B T \sum_{i=\text{hs,ion}} \rho_i(z_{\max,i}) - \frac{\sigma^2}{2\,\epsilon\,\epsilon_0}, \tag{2.6}$$

which depends on the particle densities at the plane of contact. The net pressure felt between the plates, P_{net}, is given by the difference between the internal pressure, P_{slit}, and the outside bulk pressure, $P_{\text{bulk}} = \lim_{d_{\text{wall}}\to\infty} P_{\text{slit}}$, such that

$$P_{\text{net}} = P_{\text{slit}} - P_{\text{bulk}}. \tag{2.7}$$

We use wall separations of $\sim 9 d_{\text{hs}}$ or larger to determine P_{bulk} with sufficient accuracy.

Kjellander and Marčelja [11,13] have suggested that instead of direct application of Eq. (2.6), it is desirable to transform to an equation for the midplane with the help of the Born-Green-Yvon equation. In this way the wall-wall interaction can be split into a term, P_{kin}, which depends on the midplane particle densities, and additional parts that represent pressure components due to the Coulombic and hard-core interactions (P_{el} and P_{core}, respectively) between the two fluid halves across the midplane. One has

$$\begin{aligned} P_{\text{slit}} &= P_{\text{kin}} + P_{\text{el}} + P_{\text{core}} \\ &= k_B T \sum_{i=\text{hs,ion}} \rho_i(0) - \int_0^{z_{\max,\text{ion}}} dz_1\, \rho_{\text{ion}}(z_1) \int_{-z_{\max,\text{ion}}}^{0} \\ &\quad \times dz_2\, \rho_{\text{ion}}(z_2) \int_0^{\infty} 2\pi r\, dr\, \frac{\partial u^{\text{el}}_{\text{ion ion}}(r,z_1,z_2)}{\partial z_1} \\ &\quad \times h_{\text{ion ion}}(r,z_1,z_2) \\ &\quad + k_B T \sum_{i,j=\text{hs,ion}} 2\pi \int_0^{z_{\max,i}} dz_1\, \rho_i(z_1) \int_{-z_{\max,j}}^{0} dz_2\, \rho_j(z_2) \\ &\quad \times (z_1 - z_2)\, g_{ij}(\tilde{r}_{ij}, z_1, z_2). \end{aligned} \tag{2.8}$$

The integrations over z_1 and z_2 in the last term of Eq. (2.8) are to be carried out only if $\tilde{r}_{ij}^2 = \frac{1}{4}(d_i + d_j)^2 - (z_1 - z_2)^2$ is positive. Both Eqs. (2.6) and (2.8) are exact but might yield slightly different results when applied in numerical calculations because the correlation functions are only known approximately [15]. For numerical and conceptual reasons, we use Eq. (2.8) in our calculations and will especially look at the contribution P_{el} when comparing systems with and without neutral hard-sphere solvent.

III. RESULTS

In the following discussion we refer to results for models of four types. These include the primitive model where only counterions are present between the walls, hard-sphere systems (HS) where only hard spheres occupy the slit between uncharged walls, and mixtures of counterions and hard spheres (labeled PM+HS) of particular interest here. In addition, we consider systems which are equivalent to PM+HS models except that *all* charges are switched off while keeping the number of ''ions'' between the plates fixed. We label systems of this type UCPM+HS (UC for ''uncharged'') and they prove very useful in our attempt to obtain and understand different superposition approximations for the force between the plates.

In all calculations the relevant state and interaction parameters were chosen to be consistent with $d_{\text{hs}} = 2.8$ Å, $\epsilon = 78.7$, and a temperature $T = 298$ K. Thus, the hard-sphere solvent particles are roughly the size of water molecules and the background dielectric continuum has the dielectric constant of pure water at 298 K. The walls are taken to have the same dielectric constant as the solution which circumvents the need for treating image charge effects. In fact, for the PM it has been shown [11] that image effects are not very important for the high surface charge density (-0.267 C/m^2 $= 1e/60$ Å^2) considered here. We consider divalent counterions ($q_{\text{ion}} = 2e$) with diameters $d_{\text{ion}} = d_{\text{hs}}$ and $d_{\text{ion}} = 4.25$ Å $= 1.52 d_{\text{hs}}$. The latter value is frequently used in PM calculations and is sometimes considered to represent an ''effective'' ion diameter which includes some portion of a strongly bound solvation shell. Here we have selected this value simply because it allows us to check our PM results against earlier work, and it suffices to show the large effects which occur when the ions and solvent particles differ significantly in size.

The results reported are for $\rho_{\text{hs}}^{\text{bulk}} = \lim_{d_{\text{wall}}\to\infty} \rho_{\text{hs}}(0) = 0.492/d_{\text{hs}}^3$. To achieve this value we used $a_{\text{hs}} = \gamma_{\text{hs}}^{\text{bulk}} \rho_{\text{hs}}^{\text{bulk}}$ with an activity coefficient $\gamma_{\text{hs}}^{\text{bulk}} = 57.1$. This activity coefficient differs from the corresponding ''exact'' (i.e., Carnahan-Starling) value of 40.9 due to approximations inherent in the HNC closure. We note that our bulk density is a little lower than that of water under ambient conditions (i.e., $\sim 0.7/d_{\text{hs}}$). However, the numerical solutions are dramatically easier at the lower density and the system considered is sufficiently dense to illustrate the large influence of solvent granularity which is of primary interest here. Furthermore, fluids of hard spheres are considerably more structured than waterlike models at the same density, so using a somewhat lower density offsets the ''overstructuring'' to some extent.

The presentation of the results is divided into two parts, and we first consider the simpler case where the solvent particles and ions are of the same size.

A. Equal-sized particles

In Fig. 2 we give two examples of the density profiles of hard spheres and ions in the mixture (PM+HS) and compared with the profiles for ions (PM) and hard spheres (HS) alone. Note that $\rho_i(z)$ is symmetrical around the midplane and only one-half of the profiles are shown. The most obvious feature is the tendency of the ions to be found close to the wall when the dense hard-sphere fluid is present due to entropic effects as the free space between the walls is reduced. The presence of the ions at the wall lowers the contact density of the neutral component in the mixture in comparison to the pure hard-sphere system, whereas the densities around the midplane are similar in magnitude. The profile for $d_{\text{wall}} = 3.1 d_{\text{hs}}$ plotted in Fig. 2(b) shows the appearance of maxima and minima typical of dense hard-core systems in-

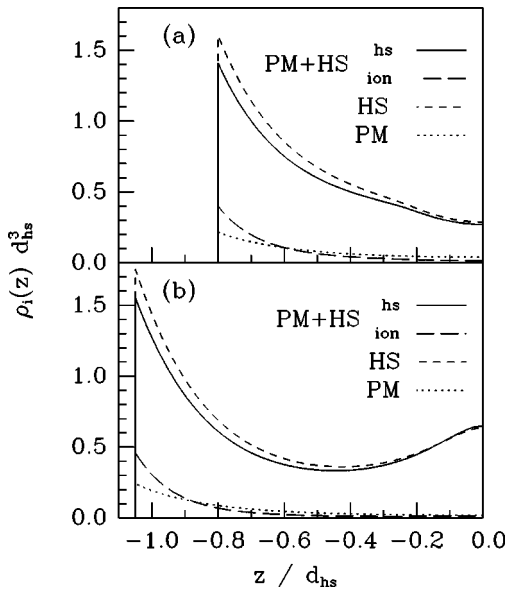

FIG. 2. Density profiles for the mixture of ions and hard spheres (PM+HS), the primitive model (PM), and the hard-sphere model (HS). In all cases $d_{ion}=d_{hs}$. In (a) $d_{wall}=2.6d_{hs}$ and in (b) $d_{wall}=3.1d_{hs}$.

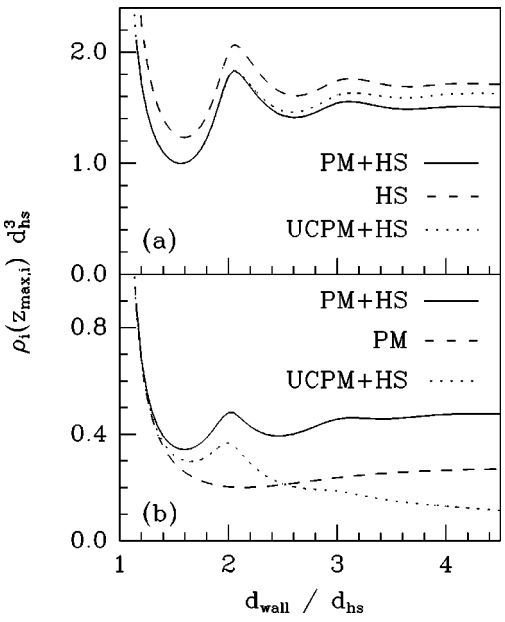

FIG. 3. Contact densities at the wall for (a) hard-sphere and (b) ion components for different models. The model labeled UCPM+HS is identical to PM+HS but the charges are switched off as described in the text. The remaining models are as in Fig. 2. In all cases $d_{ion}=d_{hs}$.

dicating the buildup of particle layers. It should be noted that with the hard-sphere bulk density used here we do not find any significant layering of the ions in contrast to the situation for $\rho_{hs}^{bulk}=0.7/d_{hs}^3$ [7,8].

An interesting point is that the total average particle density between the plates, $\overline{\rho}_{tot}$ (calculated by integrating up the density profiles of all particles for a given model), is higher for PM+HS than for HS. This fact, which is true for all wall separations, is not due to the structural changes because of the charges present. A comparison between the charged and uncharged mixtures reveals that $\overline{\rho}_{tot}$[PM+HS] and $\overline{\rho}_{tot}$[UCPM+HS] are always within 0.5% of each other, whereas $\overline{\rho}_{tot}$[HS] is up to 5% lower than the values for the binary mixtures. This indicates that the model UCPM+HS is not equivalent to HS even though all the species have identical interactions. The difference in $\overline{\rho}_{tot}$ for the pure and the mixed systems is rooted in the distinction between particles with a fixed chemical potential and particles that are located by definition (due to the electroneutrality condition) between the walls. The latter species may be viewed as part of the wall-wall system and their chemical potential is generally different from the former species even if their interactions are identical.

A more complete discussion of the trends in the density profiles is possible if we look at the contact and midplane densities as functions of d_{wall} for the different models. The contact densities (Fig. 3) for all components in the dense systems (all except the PM) show to some degree maxima (around $d_{wall}=2.05d_{hs},3.1d_{hs}$) and minima (around $d_{wall}=1.6d_{hs},2.6d_{hs}$). These are related to fluid structures that are more ''efficiently packed,'' as in Fig. 2(b), or more ''loosely packed,'' as in Fig. 2(a), respectively. At wall separations slightly larger than a multiple of d_{hs} neighboring particle layers interact more strongly and particles in the contact layer are pushed towards the wall [16]. As hard-core interactions in the PM are of no importance the corresponding curve is not structured, but has one broad minimum at $d_{wall}\approx 2.15d_{hs}$ due to correlated ion-ion density fluctuations. The midplane densities (Fig. 4) exhibit layering features similar to those of the contact values.

For $d_{wall}\lesssim 2.2d_{hs}$, the densities at the midplane and contact plane for PM+HS and UCPM+HS are very similar. This demonstrates that charge effects at these small wall separations are only of secondary importance compared with packing constraints. Features such as higher ion contact den-

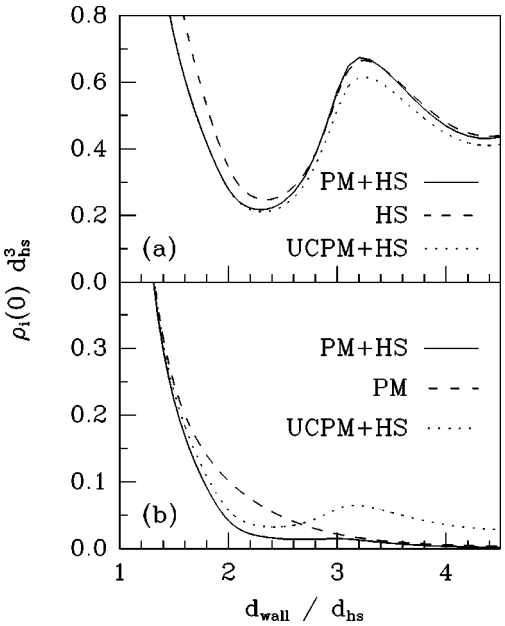

FIG. 4. Densities at the midplane for (a) hard-sphere and (b) ion components for different models. The models are as in Fig. 3. In all cases $d_{ion}=d_{hs}$.

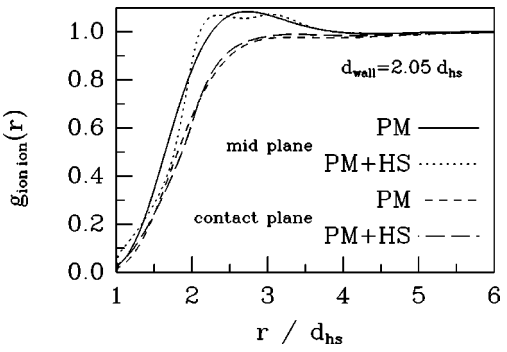

FIG. 5. $g_{\text{ion ion}}(r)$ parallel to the walls in the midplane and contact plane for the PM and PM+HS ($d_{\text{ion}}=d_{\text{hs}}$) with $d_{\text{wall}}=2.05d_{\text{hs}}$.

sities and a faster decrease of the ion midplane density with increasing d_{wall} for the PM+HS compared to the PM come about because of the hard-core interactions. For larger wall separations the curves for the charged and uncharged mixtures deviate significantly. The ''ions'' in the UCPM+HS spread more evenly over the accessible space and their contact density falls slowly to zero as d_{wall} increases, whereas a constant nonzero contact density is reached for the PM+HS [see Fig. 3(b)].

The solution of the integral equations also yields the particle distribution functions g_{ij}. These functions depend on three coordinates and are therefore hard to depict, especially if small differences between models are to be shown. Here (Fig. 5), we present only a plot of $g_{\text{ion ion}}(r)$ parallel to the wall at the contact plane and midplane for $d_{\text{wall}}=2.05d_{\text{hs}}$. The differences between the $g_{\text{ion ion}}(r)$ for the PM and the mixture are rather small (i.e., <0.1). This means that, although the average positioning of the ions between the plates (as indicated by the density profiles) changes considerably upon insertion of the hard spheres, the ion-ion structure in the fluid is not disturbed very much. The presence of the hard-sphere solvent induces small undulations with a ''wavelength'' slightly smaller than the solvent diameter, similar to the effects produced by a more realistic solvent model in bulk solution [3]. For the PM midplane function, the single maximum at $r=2.7d_{\text{hs}}$, which constitutes the global maximum as well [as seen in a full two-dimensional contour plot], is split into two maxima in the mixture. The oscillations in $g_{\text{ion ion}}(r)$ in the contact plane are smaller and no maximum exists; the global maximum (and the most probable spot for the next ion) can be found at the opposite wall.

We now discuss the pressure perpendicular to the walls. Because of the contact theorem [Eq. (2.6)], most of the points raised in our discussion of the behavior of the contact densities hold for the pressure as well. Figure 6(a) shows the oscillating pressure for the pure hard-sphere system together with the smooth, slightly attractive curve for the PM and the electrostatic component, P_{el}, calculated via Eq. (2.8). P_{el} is always attractive and arises because of correlated ion-ion fluctuations across the midplane (i.e., it is zero for Poisson-Boltzmann-like theories which ignore these correlations). The net pressure for the system of interest, PM+HS, together with results given by two superposition approximations, is plotted in Fig. 6(b). If one wishes to estimate P_{net} for PM+HS with simple addition schemes involving more basic

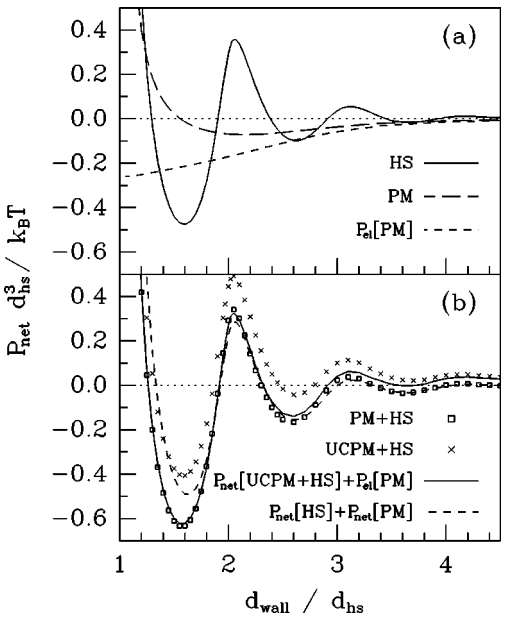

FIG. 6. The net pressure acting between the plates obtained for the different models and with different superposition approximations. In all cases $d_{\text{ion}}=d_{\text{hs}}$. The labels are as in Fig. 3 and as discussed in the text.

components, different possibilities are available. The simplest suggestion is to add the values of P_{net} for the pure systems (i.e., $P_{\text{net}}[\text{HS}]+P_{\text{net}}[\text{PM}]$). From Fig. 6(b), we see that for the equal-sized case this gives good agreement down to $d_{\text{wall}}\approx 1.8d_{\text{hs}}$.

For small wall separations another procedure yields much better values, specifically, the superposition of $P_{\text{net}}[\text{UCPM+HS}]$ and $P_{\text{el}}[\text{PM}]$. The idea leading to this choice is that for small wall separations packing effects are crucial for the fluid structure and should be separated from the electrostatic contribution. P_{el}, on the other hand, shows rather small changes when comparing ion models with and without hard spheres (as is evident from Fig. 7) despite significant differences in the density profiles. However, this superposition scheme breaks down at larger wall separations as the ''ions'' in UCPM+HS do not stay close to the walls (as do those in PM+HS) and the pressure is systematically overestimated.

A couple of remarks are appropriate here. First, the comparisons made in the preceding paragraphs are of rather aca-

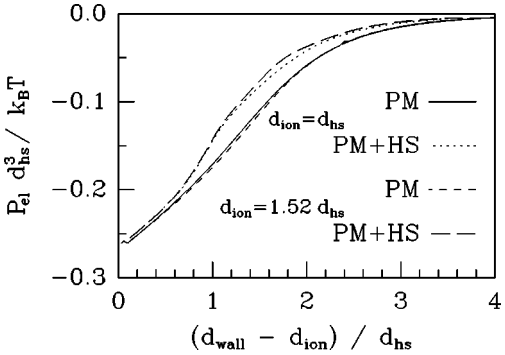

FIG. 7. The electrostatic component of the pressure for the PM and PM+HS. Results for $d_{\text{ion}}=d_{\text{hs}}$ and for $d_{\text{ion}}=1.52d_{\text{hs}}$ are shown.

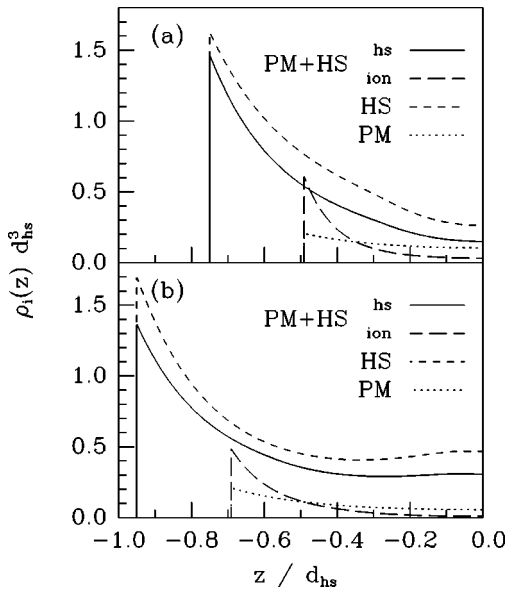

FIG. 8. Density profiles for the mixture of ions and hard spheres (PM+HS), the primitive model (PM), and the hard-sphere model (HS). In all cases $d_{ion}=1.52d_{hs}$. In (a) $d_{wall}=2.5d_{hs}$ and in (b) $d_{wall}=2.9d_{hs}$.

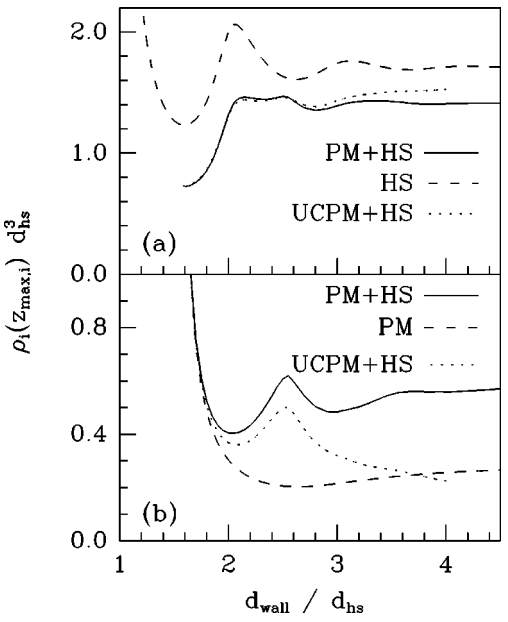

FIG. 9. Contact densities at the wall for (a) hard-sphere and (b) ion components for different models. The models are as in Fig. 3. In all cases $d_{ion}=1.52d_{hs}$.

demic interest as we do not suggest that any procedure of adding pressure components of different models will yield exactly $P_{net}[\mathrm{PM+HS}]$. Further, because of the restriction to equal-sized particles, most schemes of combining the oscillating pressure found for the hard-sphere fluid with a slight attraction of electrostatic origin will likely give a fair qualitative picture. The case where the ions and solvent particles are of unequal size considered in the following subsection is much more interesting. Secondly, note that $P_{net}[\mathrm{HS}]$ and $P_{net}[\mathrm{UCPM+HS}]$ are not the same although the ''ions'' and hard spheres are identical in UCPM+HS. This is due to the above-mentioned peculiarity of the present model, where the bulk is treated as a pure fluid with the mixture existing only in the cavity between the walls.

B. Larger ions

A set of calculations analogous to those described above have been performed for systems with identical diameters for the neutral hard-sphere component, but with ions which are 50% larger, or, more precisely, $d_{ion}=4.25$ Å$=1.52d_{hs}$. With this choice, the ions are considerably larger than the solvent particles and deviations from the equal-sized case are expected to be significant. Moreover, this value of d_{ion} is often used in studies of the PM and results for the pure ion system have been published [2]. We note that for both ion sizes considered here the PM yields essentially identical results (with the appropriate redefinition of d_{wall}); the divalent counterions stay sufficiently apart from each other that ion-ion hard-core interactions are not important. See, for example, the P_{el} plots given in Fig. 7. For larger values of d_{ion} and especially for monovalent ions [2] density profiles and pressure curves depend more strongly on the ion diameter.

A qualitative comparison of Figs. 8 and 2 indicates that with the different particle sizes the density profiles differ more significantly from those of the pure systems. This comes about because an ''in phase'' layering of ions and hard-sphere solvent particles is no longer possible. The incommensurate diameters appear to bring on an even more pronounced tendency to push the ions towards the walls. The plot of the contact densities given in Fig. 9 confirms this observation; the ion contact densities are higher and those of the neutral species lower compared to the mixture with particles of the same size (Fig. 3). Another point of interest is that the first maximum of the ion contact density in the mixture (PM+HS) is at $d_{wall}\approx 2.5d_{hs}=d_{hs}+d_{ion}$, which means that ions are pushed closer to one wall by hard spheres associated with the contact layer at the opposite wall. The pure hard-sphere fluid (HS) has its first maximum slightly higher than $d_{wall}=2d_{hs}$ [Fig. 9(a)]. Since hard spheres in PM+HS and UCPM+HS are affected by the interactions with both species at the opposite wall we find two maxima at the corresponding wall separations for these mixtures.

This more complex behavior can also be found for the pressure between the walls shown in Fig. 10. The distances between maxima and minima in P_{net} for PM+HS are irregular and no correlation with the oscillations characteristic of the HS model is apparent. The curves shown in Fig. 10(b) also demonstrate that the simple addition approximation $P_{net}[\mathrm{PM+HS}]\approx P_{net}[\mathrm{HS}]+P_{net}[\mathrm{PM}]$ is not good at any wall separation if the particle diameters are sufficiently different. On the other hand, the more complicated scheme, $P_{net}[\mathrm{PM+HS}]\approx P_{net}[\mathrm{UCPM+HS}]+P_{el}[\mathrm{PM}]$, works very well for smaller values of d_{wall}. Deviations do occur at larger wall-wall separations where the fluid structure in UCPM+HS differs significantly from that of PM+HS. Nevertheless, these results show that to a good approximation the net pressure in the PM+HS can be viewed as a superposition of an attractive electrostatic part and a ''quasioscillatory'' component arising from the hard-core interactions in the system.

IV. SUMMARY AND CONCLUSIONS

We have solved the anisotropic HNC approximation for mixtures of neutral hard spheres and divalent counterions

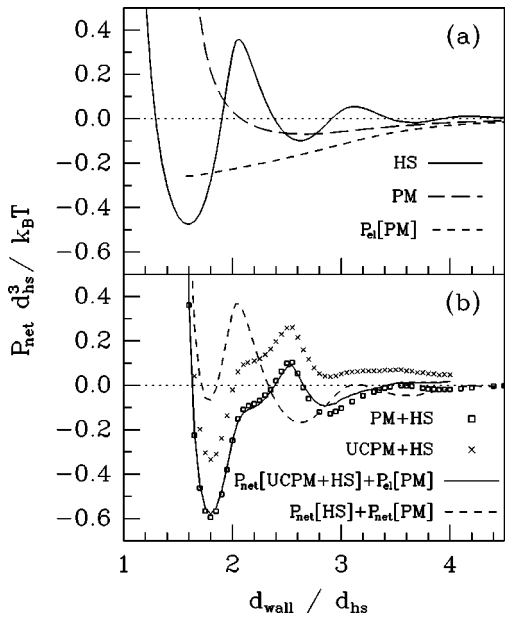

FIG. 10. The net pressure acting between the plates obtained for the different models and with different superposition approximations. In all cases $d_{ion}=1.52d_{hs}$. The labels are as in Fig. 3 and as discussed in the text.

between charged hard walls. In agreement with earlier calculations [8,10], we observe that adding a neutral solvent to the PM modifies the ion density profiles considerably. The hard-core ion-solvent interactions tend to push the ions towards the wall, resulting in higher ion densities at contact. This effect is amplified if the ions are larger than the solvent particles.

We find that, even at moderate solvent density and high surface charge density, the net pressure between the walls at separations of a few solvent diameters tends to be largely dominated by oscillations associated with the hard-core interactions. At these separations electrostatic effects are only of secondary importance in these models. For the restrictive case where the ions and solvent particles are of the same size the oscillations are regular and similar to those for a pure hard-sphere fluid. For this system, simply adding the PM and hard-sphere pressures gives a reasonable approximation to the forces found for the mixture. If the ions and solvent particles are significantly different in size, one obtains a more complex pressure curve which cannot be approximated by simply adding the PM and hard-sphere pressures. However, for wall separations up to several solvent diameters the net pressure can still be well described by a better superposition approximation. This consists of adding the net pressure for a corresponding uncharged hard-sphere mixture to the purely electrostatic component, P_{el}, of the PM. This scheme works because the hard-core interactions remain the most important contribution and the P_{el} component in the mixture differs little from that of the PM.

In conclusion, this work along with earlier studies strongly suggests that in real solutions, solvent effects not included in the PM are likely more important than the ionic interactions in determining the force between charged plates at separations of a few solvent (or ion) diameters. Furthermore, we have shown that simple superposition of ionic and solvent pressures only works if the ions and solvent particles are of similar size. A more accurate superposition scheme can be devised but, although it provides physical insight into the nature of the forces involved, its application is not particularly practical. We are currently investigating solvent effects which arise from reduced dielectric screening as discussed in the Introduction. Our preliminary work indicates that these too can have significant consequences for the force acting between charged plates.

ACKNOWLEDGMENT

The financial support of the National Science and Engineering Research Council of Canada is gratefully acknowledged.

[1] R. Kjellander, Ber. Bunsenges. Phys. Chem. **100**, 894 (1996), and references therein.
[2] R. Kjellander, T. Åkesson, B. Jönsson, and S. Marčelja, J. Chem. Phys. **97**, 1424 (1992).
[3] P. G. Kusalik and G. N. Patey, J. Chem. Phys. **88**, 7715 (1988); **89**, 5843 (1988).
[4] P. G. Kusalik and G. N. Patey, J. Chem. Phys. **89**, 7478 (1988).
[5] R. Kjellander, S. Marčelja, R. M. Pashley, and J. P. Quirk, J. Phys. Chem. **92**, 6489 (1988); J. Chem. Phys. **92**, 4399 (1990).
[6] S. Marčelja, Biophys. J. **61**, 1117 (1992).
[7] L. Zhang, H. T. Davis, and H. S. White, J. Chem. Phys. **98**, 5793 (1993).
[8] Z. Tang, L. E. Scriven, and H. T. Davis, J. Chem. Phys. **97**, 494 (1992).
[9] Z. Tang, L. E. Scriven, and H. T. Davis, J. Chem. Phys. **100**, 4527 (1994).
[10] C. N. Patra and S. K. Ghosh, Phys. Rev. E **49**, 2826 (1994).
[11] R. Kjellander and S. Marčelja, Chem. Phys. Lett. **112**, 49 (1984).
[12] R. Kjellander and S. Marčelja, J. Chem. Phys. **82**, 2122 (1985).
[13] R. Kjellander and S. Marčelja, Chem. Phys. Lett. **127**, 402 (1986).
[14] R. Kjellander, J. Chem. Phys. **88**, 7129 (1988); **89**, 7649 (1988).
[15] R. Kjellander and S. Sarman, Mol. Phys. **70**, 215 (1990).
[16] R. Kjellander and S. Sarman, J. Chem. Soc., Faraday Trans. **87**, 1869 (1991).
[17] We use the orthogonal Hankel transform proposed by Lado: F. Lado, J. Comput. Phys. **8**, 417 (1971).
[18] S. L. Carnie and D. Y. C. Chan, J. Chem. Phys. **74**, 1293 (1981); also see D. Henderson and L. Blum, *ibid.* **75**, 2025 (1981).